

Kondo lattices with inequivalent local moments: Competitive vs. co-operative Kondo screening

Adel Benlagra,¹ Lars Fritz,² and Matthias Vojta¹

¹*Institut für Theoretische Physik, Technische Universität Dresden, 01062 Dresden, Germany*

²*Institut für Theoretische Physik, Universität zu Köln, Zùlpicher Straße 77, 50937 Köln, Germany*

(Dated: January 13, 2013)

While standard heavy fermion metals feature a single spin-1/2 local moment per unit cell, more complicated systems with multiple *distinct* local moments have been synthesized as well, with $\text{Ce}_3\text{Pd}_{20}(\text{Si,Ge})_6$ being one example. Here, we discuss the physics of a Kondo lattice model with two local-moment sublattices, coupled with different Kondo couplings to conduction electrons. The phase diagram will be strongly modified from that of the standard Kondo lattice if the characteristic screening temperatures of the distinct moments are well separated. Therefore, we investigate the interplay between the two Kondo effects using a local self-energy approximation via slave bosons. We find that the two Kondo effects can either compete or co-operate depending on the conduction-band filling. In the regime of competition, small differences in the two Kondo couplings can lead to huge differences in the respective Kondo scales, due to non-trivial many-body effects. We also study the low-temperature properties of the collective heavy Fermi-liquid state and propose a connection to depleted Kondo lattice systems.

PACS numbers: 71.27.+a, 72.15.Qm, 75.20.Hr, 75.30.Mb

I. INTRODUCTION

Inter-metallic compounds containing rare-earth ions have been the subject of intense experimental and theoretical efforts, owing to their fascinating physical properties. These include heavy fermion mass enhancement, unconventional magnetism and superconductivity, non-Fermi liquid behavior as well as the exciting possibility of quantum criticality beyond the Landau-Ginzburg-Wilson paradigm.^{1–3} Microscopically, most systems contain one rare-earth ion per unit cell, with a single unpaired f electron or hole, lending themselves to a theoretical description in terms of a Kondo lattice model with one spin-1/2 local moment per unit cell.

Recent work^{4–6} on the family of ternary compounds $(\text{RE})_3\text{Pd}_{20}\text{X}_6$ (Re=rare-earth, X=Si, Ge), which feature *two* inequivalent Kondo sites per unit cell,^{7–9} uncovered a variety of interesting phenomena. Upon cooling, two magnetic phase transitions occur.^{10–12} In $\text{Ce}_3\text{Pd}_{20}\text{Si}_6$, regarded as one of the heaviest electron Kondo systems with a low-temperature specific-heat coefficient of $C/T = 8 \text{ J/mol Ce K}^2$, the lower transition can be tuned to zero temperature by application of a magnetic field, resulting in non-Fermi liquid signatures with a linear temperature dependence of the resistivity.^{13,14} Furthermore, substitution studies^{6,15} suggest that quantum criticality might also be achieved by pressure. Together, these results call for theoretical investigations of Kondo lattices with multiple Kondo ions.

A. General considerations

Theoretically, little is known about the behavior of Kondo lattices with multiple distinct local moments per unit cell. Here we start with a few general considerations

for a system with two distinct Kondo ions.

For sufficiently strong Kondo couplings, a paramagnetic Fermi liquid phase with fully screened moments can be expected. Its Fermi volume is given by $\mathcal{V}_{\text{FL}} = K_d(n_{\text{tot}} \bmod 2)$ with $n_{\text{tot}} = 2n_c + 2n_f = 2n_c + 2$, where $2n_c$ and $2n_f$ denote the average number of c and f electrons per unit cell, respectively. Further, $K_d = (2\pi)^d/(2v_0)$ is a phase space factor, with v_0 the unit cell volume and the factor of two accounting for the spin degeneracy of the bands. If, in contrast, inter-moment interactions dominate, phases with magnetic long-range order (LRO, e.g. antiferromagnetic) without Kondo screening appear natural; alternatively, inter-moment singlet formation of spin-Peierls type can also occur. Given two spin-1/2 moments per crystallographic unit cell (more generally, an even number), both phases can be realized without further lattice symmetry breaking, resulting in a Fermi volume $\mathcal{V}_{\text{AF}} = K_d(2n_c \bmod 2)$ which equals \mathcal{V}_{FL} .

Interestingly, a novel regime with *partial* Kondo screening may be reached when the characteristic Kondo scales of the two ions are distinctly different. First, upon increasing the temperature in the paramagnetic Fermi liquid, the magnetic entropy will be released in two stages, allowing to define two “screening” temperatures T_1 and T_2 associated with the two ions. Second, upon increasing inter-moment interactions at low temperature, magnetically ordered phases can occur, where one set of moments is strongly polarized with little screening, while the second set of moments still forms heavy quasiparticles with weak polarization. Such a magnetic phase is – apart from the possibility of Lifshitz transitions associated with changes in the Fermi-surface topology – continuously connected to a local-moment metallic magnet without Kondo screening,¹⁶ but observables will reflect the co-existence of local-moment magnetism with heavy fermion behavior. A schematic phase diagram

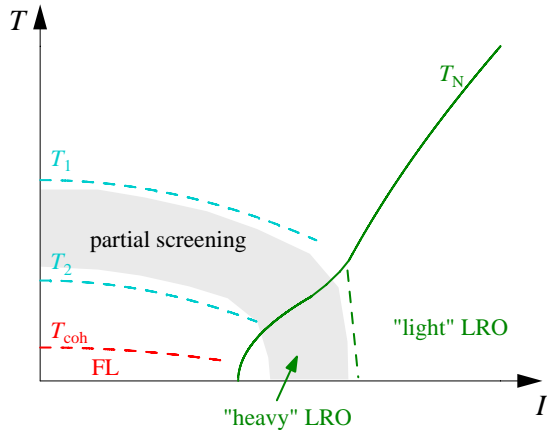


FIG. 1: Schematic phase diagram of a Kondo lattice with two inequivalent local moments per unit cell, as function of temperature T and the magnitude of the inter-moment exchange I (measured relative to a microscopic Kondo scale, e.g., the largest single-ion Kondo temperature of the system). The crossover temperatures $T_{1,2}$ mark the high-temperature onset of screening of the two ions in their lattice environment, while T_{coh} is the lattice coherence scale below which the system displays Fermi-liquid behavior. Partial Kondo screening is realized for $T_2 < T < T_1$ (shaded). Upon increasing I , the system enters a long-range-ordered (e.g. antiferromagnetic) phase where the order is mainly carried by the low- T_K ions (here “2”), while the high- T_K ions (“1”) remain almost fully screened – this is a “heavy LRO” phase. Further increasing I induces a crossover into a more conventional regime where all moments participate in the order (“light LRO”). It is conceivable that the “light” and “heavy” LRO regimes are characterized by different ordering patterns, necessitating further phase transitions inside the LRO phase. The focus of this paper is on the regime of small I .

resulting from this discussion, which extends Doniach’s considerations¹⁷ to the case of multiple distinct Kondo ions, is shown in Fig. 1.

A central question is then under which conditions the two screening scales T_1 and T_2 will be vastly different. On the one hand, this of course depends on bare model parameters (i.e. the Kondo couplings and local densities of states), but – on the other hand – there is room for mutual influence and non-trivial interplay of the screening processes. The latter can be phrased into the following question: Does the onset of Kondo screening for one set of moments at some temperature T_1 promote or inhibit the screening of the second set of moments? Naive arguments can be found for either scenario: If the main effect of the higher-temperature Kondo screening is to inject additional states near the Fermi level, then the lower-temperature Kondo effect should be boosted.¹⁸ Alternatively, a variant of the exhaustion argument¹⁹ would imply that, once the higher-temperature Kondo effect sets in, fewer conduction electrons are left available for the lower-temperature Kondo effect, which is then inhibited. In the latter scenario, small differences in the two Kondo

couplings can cause largely different $T_{1,2}$. Naturally, the lower of the two screening temperatures $T_{1,2}$ sets an upper bound to the low-temperature coherence scale T_{coh} of the heavy Fermi liquid (experimentally often defined as the upper boundary of T^2 behavior in the resistivity). However, even for standard Kondo lattices with one local moment per unit cell it has been shown^{20–22} that T_{coh} can be tiny compared to the onset temperature of screening (provided that inter-site effects are negligible²⁴), in particular in the so called “exhaustion regime” of small band filling. Clearly, the issue of what determines the coherence scale T_{coh} in the case of multiple distinct local moments is far from obvious.

The purpose of this paper is to tackle the simplest set of questions outlined above, namely that of screening and coherence scales in the heavy Fermi-liquid regime of a Kondo lattice model with two distinct local moments. These issues can be efficiently addressed in a local self-energy approximation using slave bosons.^{23,24} We shall discuss the interplay between the Kondo crossovers of the two sets of moments. As detailed below, we find that – depending on the conduction-band filling n_c – the Kondo processes may either compete or co-operate. For both cases, we describe the consequences for the low-temperature behavior and discuss experimental implications. In particular, we shall argue that small conduction-band filling tends to open a window of partial Kondo screening as in Fig. 1. Further, the dominant influence of the conduction-band filling furnishes a link between the problem studied here and a seemingly different one, namely a Kondo lattice with random depletion of local moments.^{25–27}

We note that partial Kondo screening, somewhat similar to the regime advertised in Fig. 1, has been predicted to occur in certain frustrated Kondo lattices, where a spontaneous modulation of the Kondo effect is instrumental in releasing geometric frustration.^{28,29}

B. Outline

The remainder of this paper is organized as follows. In Sec. II we introduce the microscopic Kondo lattice model with two distinct Kondo ions, to be studied in this paper. This model is studied in the framework of the slave-boson mean-field approach. The emergent Kondo scales are derived and discussed in Sec. III, including the physical picture of competing vs. co-operating Kondo effects. The low-temperature properties of the Fermi liquid are the subject of Sec. IV. We shall conclude by relating our results to depleted-Kondo-lattice physics and by discussing directions for future work. Technical details are relegated to the appendices.

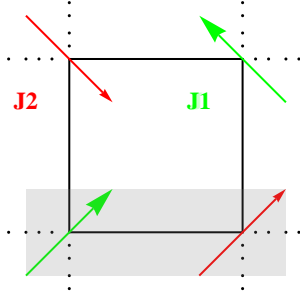


FIG. 2: Sketch of a lattice described by the model (1). Two types of local moments are coupled to the conduction electrons of the two sublattices with Kondo couplings $J_{1,2}$. The shaded area defines the unit cell including two spin-1/2 local moments. Dots symbolize translation symmetry.

II. MODEL AND MEAN-FIELD APPROXIMATION

In the body of this paper, we discuss a Kondo lattice model with two inequivalent local-moment sublattices, with a Hamiltonian of the form

$$\mathcal{H} = - \sum_{\langle i,j \rangle, \sigma} t_{ij} c_{i\sigma}^\dagger c_{j\sigma} + \sum_i J_i \vec{S}_i \cdot \vec{s}_i - \mu \sum_{i\sigma} \left(c_{i\sigma}^\dagger c_{i\sigma} - n_c \right), \quad (1)$$

in standard notation, with $\vec{s}_i = \sum_{\sigma\sigma'} c_{i\sigma}^\dagger \vec{\tau}_{\sigma\sigma'} c_{i\sigma'}/2$ being the spin density of conduction electrons at site i and n_c the average number of c electrons per site. The lattice, with a total number of unit cells \mathcal{N} , is assumed to be bi-partite with sublattices A and B. The Kondo coupling J_i differs for both sublattices and is given by

$$J_i = J_1 \delta_{iA} + J_2 \delta_{iB} \quad (2)$$

where $\delta_{i\alpha} = 1$ (0) for $i \in \alpha$ ($i \notin \alpha$) and $\alpha = A, B$. In the following, we will assume $J_1 \geq J_2$.

The unit cell of the model (1) contains two c orbitals and two local-moment (or f) orbitals, Fig. 2. For most of the paper, we shall consider simple nearest-neighbor hopping only, such that $t_{ij} = t$ on nearest-neighbor bonds and $t_{ij} = 0$ otherwise. Both longer-range hopping and additional kinetic-energy modulations (compatible with the lattice symmetry) are not expected to qualitatively change our conclusions; this is explicitly shown in Appendix B for the case of a square lattice with second-neighbor hopping. For $J_1 = J_2$ our model reduces to the standard Kondo lattice with conduction electron filling n_c , dubbed “homogeneous” case in the following.

A. Slave-boson mean-field approximation

The model (1) will be tackled using a standard slave-boson technique. We use a fermionic representation for the local spin \vec{S}_i , introducing auxiliary fermions $f_{i\sigma}$ such

that

$$\vec{S}_i = \sum_{\sigma\sigma'} f_{i\sigma}^\dagger \vec{\tau}_{\sigma\sigma'} f_{i\sigma'}/2,$$

together with a local constraint $\sum_{\sigma} f_{i\sigma}^\dagger f_{i\sigma} = 1$. The Kondo interaction in (1) now takes the form

$$\mathcal{H}_K = -\frac{1}{2} \sum_{i,\sigma\sigma'} J_i f_{i\sigma}^\dagger c_{i\sigma} c_{i\sigma'}^\dagger f_{i\sigma'}, \quad (3)$$

where additional terms have can be absorbed into chemical potential and have been thus dropped. The interaction (3) is then decoupled using a field b_i conjugate to $(\sum_{\sigma} \sqrt{J_i} f_{i\sigma}^\dagger c_{i\sigma})$. The Lagrangian then reads

$$\begin{aligned} \mathcal{L} = & T \sum_{i,j,\omega,\sigma} \left(-(i\omega + \mu) \delta_{ij} - t_{ij} \right) c_{i\sigma}^\dagger c_{j\sigma} - \sum_{i,\sigma} \lambda_i f_{i\sigma}^\dagger f_{i\sigma} \\ & + \sum_{i,\sigma} \sqrt{J_i} \left(f_{i\sigma}^\dagger c_{i\sigma} b_i + H.c. \right) + \sum_i \left(2b_i^\dagger b_i + \lambda_i \right) + 2\mathcal{N} n_c \mu \end{aligned} \quad (4)$$

Recall that \mathcal{N} is the number of two-site unit cells of the lattice.

The mean-field theory is obtained from the Lagrangian (4) by assuming that the fields b and λ have uniform and static expectation values on each sublattice

$$\langle b_{i\alpha} \rangle = b_\alpha, \quad \langle \lambda_{i\alpha} \rangle = \lambda_\alpha.$$

The approximation (5) is formally exact in the $N \rightarrow \infty$ limit of a model with the spin symmetry extended to $SU(N)$.

Performing a Fourier transformation, $c_{\mathbf{k}\sigma\alpha}(f_{\mathbf{k}\sigma\alpha}) = \frac{1}{\sqrt{\mathcal{N}}} \sum_{j \in \alpha} e^{i\mathbf{k} \cdot \mathbf{x}_j} c_{j\sigma}(f_{j\sigma})$, \mathbf{k} running over the Brillouin zone of the Bravais lattice, one obtains the following mean-field Lagrangian

$$\begin{aligned} \mathcal{L} = & -\frac{T}{\mathcal{N}} \sum_{\alpha,\beta} \sum_{\mathbf{k},\mathbf{q},\omega,\sigma} \left(c_{\mathbf{k}\sigma\alpha}^\dagger f_{\mathbf{k}\sigma\alpha}^\dagger \right) \mathcal{G}_{\alpha\beta}^{-1}(i\omega, \mathbf{k}) \begin{pmatrix} c_{\mathbf{k}\sigma\beta} \\ f_{\mathbf{k}\sigma\beta} \end{pmatrix} \\ & + 2\mathcal{N} \sum_{\alpha} b_{\alpha}^2 + \mathcal{N} \sum_{\alpha} \lambda_{\alpha} + 2\mathcal{N} n_c \mu, \end{aligned} \quad (5)$$

where the 4×4 inverse Green’s function matrix \mathcal{G}^{-1} is defined by

$$\mathcal{G}_{\alpha\beta}^{-1}(i\omega, \mathbf{k}) = \begin{pmatrix} (i\omega + \mu) \delta_{\alpha\beta} - \mathcal{E}_{\alpha\beta}(\mathbf{k}) & -\sqrt{J_\alpha} b_\alpha \delta_{\alpha\beta} \\ -\sqrt{J_\alpha} b_\alpha \delta_{\alpha\beta} & (i\omega + \lambda_\alpha) \delta_{\alpha\beta} \end{pmatrix}, \quad (6)$$

and

$$\mathcal{E}(\mathbf{k}) = \begin{pmatrix} \zeta_{\mathbf{k}} & \epsilon_{\mathbf{k}}^* \\ \epsilon_{\mathbf{k}} & \xi_{\mathbf{k}} \end{pmatrix} \quad (7)$$

is the kinetic-energy matrix whose diagonal (off-diagonal) elements result from intra- (inter-) sublattice hopping.

The mean-field free energy is readily obtained from (5) as

$$F_{MF} = -T \text{Tr} \log(-\mathcal{G}^{-1}) + 2\mathcal{N} \sum_{\alpha} b_{\alpha}^2 + \mathcal{N} \sum_{\alpha} \lambda_{\alpha} + 2\mathcal{N} n_c \mu, \quad (8)$$

where Tr is a trace over all internal indices $\alpha, \mathbf{k}, \omega, \sigma$.

Self-consistent mean-field equations are obtained by minimizing the free energy (8) with respect to b_{ν} , λ_{ν} and μ . The result is:

$$\begin{aligned} b_{\nu} &= \frac{T\sqrt{J_{\nu}}}{\mathcal{N}} \sum_{\mathbf{k}, \omega} \mathcal{G}_{\nu\nu}^{fc}(i\omega, \mathbf{k}), \\ 1 &= \frac{2T}{\mathcal{N}} \sum_{\mathbf{k}, \omega} \mathcal{G}_{\nu\nu}^{ff}(i\omega, \mathbf{k}) e^{i\omega 0^+}, \\ n_c &= \frac{n_{c1} + n_{c2}}{2}, \end{aligned} \quad (9)$$

where the average occupation number of the c band on each sublattice is given by

$$n_{c\nu} = \frac{2T}{\mathcal{N}} \sum_{\mathbf{k}, i\omega} \mathcal{G}_{\nu\nu}^{cc}(i\omega, \mathbf{k}) e^{i\omega 0^+}. \quad (10)$$

Here \mathcal{G}^{cc} , \mathcal{G}^{ff} and \mathcal{G}^{fc} are the 2×2 sub-matrices of \mathcal{G} , corresponding to the c , f and mixed sectors, respectively. The factors of two in the occupation numbers arise from summation over spin.

In the slave-boson mean-field approximation, the original problem has thus been mapped onto a model of *four* bands with inequivalent hybridization $\sqrt{J_{\alpha}} b_{\alpha}$ between the c_{α} and f_{α} bands. The resulting renormalized bands are defined by their dispersions $E_{\mathbf{k}m}$, $m = 1, 2, 3, 4$, solutions of the eigenvalue problem

$$\text{Det } \mathcal{G}^{-1}(E_{\mathbf{k}}, \mathbf{k}) = 0. \quad (11)$$

While it is not possible, in general, to obtain a closed form for the solution of (11), simplifications arise upon considering inter-sublattice (e.g. nearest-neighbor) hopping only, such that $\zeta_{\mathbf{k}} = \xi_{\mathbf{k}} = 0$. Further, if sublattice modulations of the hopping are absent, $\epsilon_{\mathbf{k}}$ is real, and the c -electron kinetic energy is given by $\pm\epsilon_{\mathbf{k}}$. In this case, one can invert the relation $E \equiv E_m(\epsilon_{\mathbf{k}})$ and write

$$\epsilon(E) = \sqrt{\prod_{\nu=1}^2 \frac{J_{\nu} b_{\nu}^2 - (\lambda_{\nu} + E)(\mu + E)}{\lambda_{\nu} + E}}. \quad (12)$$

In particular, at the Fermi level, $E = 0$, we have

$$\mu_L \equiv \epsilon(0) = \sqrt{\prod_{\nu=1}^2 \left(\frac{J_{\nu} b_{\nu}^2}{\lambda_{\nu}} - \mu \right)}. \quad (13)$$

μ_L may be interpreted as a c -band chemical potential accounting for the enlargement of the Fermi volume due to

the Kondo effect, see Eq. (A3). In our case, $b_1, b_2 \neq 0$ at $T = 0$, and the resulting Fermi volume \mathcal{V}_{FL} encompasses $(2n_c + 2) \bmod 2$ electrons.

In the mean-field equations, the restriction to inter-sublattice hopping only allows one to convert the momentum summations into energy integrals

$$\frac{1}{\mathcal{N}} \sum_{\mathbf{k}} \dots \rightarrow \int d\omega \rho_0(\omega) \dots,$$

where $\rho_0(\omega)$ is the bare density of states (DOS) of the conduction electrons,

$$\rho_0(\omega) \equiv 1/\mathcal{N} \sum_{\mathbf{k}} [\delta(\omega - \epsilon_{\mathbf{k}}) + \delta(\omega + \epsilon_{\mathbf{k}})]. \quad (14)$$

The DOS is symmetric, $\rho_0(\omega) = \rho_0(-\omega)$, due to $\zeta_{\mathbf{k}} = \xi_{\mathbf{k}} = 0$. Note that without sublattice modulations of the bare kinetic energy, ρ_0 is identical to the bare local c -electron DOS on both sublattices A and B.

In the following, the equations assume nearest-neighbor hopping only. To ease the numerical implementation, the following calculations have been performed with either a semi-elliptic DOS, corresponding to a Bethe lattice with nearest-neighbor hopping, or a constant DOS, with no qualitative differences regarding the interplay between the two Kondo effects. In addition, we show some results for a square lattice, with and without next-neighbor hopping, in Appendix B.

Finally, we note that non-local two-particle effects are not included in the present slave-boson approximation. In particular, there are no correlations between different local-moment spins, i.e., effects of RKKY interaction are neglected. At the mean-field level, this can be (partially) repaired by explicitly adding an inter-moment interaction which is then decoupled in the particle-particle or particle-hole channel. Such a procedure can, e.g., account for a spin-liquid phase competing with Kondo screening, but this is left for a future study.

III. KONDO SCALES

Let us start by recalling a few features of the slave-boson approximation applied to Kondo physics. The onset of Kondo screening is in general signaled by an (artificial) phase transition: For $T > T_K$, the mean field b vanishes while it is non-zero for $T < T_K$. For a single Kondo impurity coupled by an exchange coupling J to a bath with a DOS $\rho_0(\omega)$, the mean-field Kondo temperature $T_K(J)$ is the solution of

$$\frac{2}{J} = \int_{-\infty}^{+\infty} d\omega \frac{\rho_0(\omega + \mu)}{\omega} \tanh\left(\frac{\omega}{2T_K}\right). \quad (15)$$

For a constant DOS and in the weak-coupling limit, $T_K(J)$ evaluates to

$$T_K(J) \sim \sqrt{D^2 - \mu^2} \exp[-1/(J\rho_0)]. \quad (16)$$

Compared to the exact single-ion Kondo temperature, $T_K^{(1)}$, this mean-field T_K has the correct exponential dependence on J and ρ_0 , and the prefactor matches the one-loop result for $T_K^{(1)}$. The artificial phase transition at $T_K(J)$ will turn into the physically correct crossover upon including gauge fluctuations in the slave-particle description.

Remarkably, the slave-boson approximation applied to a standard Kondo lattice, with bare c electron DOS $\rho_0(\omega)$ and Kondo coupling J , leads to an onset of screening at exactly the same $T_K(J)$, simply because c electrons and local moments are decoupled for $T > T_K(J)$. However, coherent Fermi-liquid behavior may set in at a much lower temperature T_{coh} (even at the mean-field level), due to protracted screening.²⁰

With two inequivalent ions, there will be two onset temperatures for screening, T_1 and T_2 , i.e., upon increasing the temperature the mean field parameter b_ν will vanish at the temperature T_ν . From $J_1 > J_2$ we expect $T_1 > T_2$. The regime $T > T_1$ consists of conduction electron decoupled from all local moments – this is a perturbative high-temperature regime. When $T_2 < T < T_1$, the local moments on sublattice A are hybridized with the c electrons, while those on B are free – this is the regime of partial screening advertised in the introduction. Finally, below T_2 , all local moments are hybridized. As above, the coherence scale T_{coh} , to be discussed in Sec. IV, may be significantly below T_2 .

A. Two-stage screening

The Kondo scales T_1, T_2 are readily obtained from the mean-field equations (9) in the limits $b_1 \rightarrow 0$, $b_2 \rightarrow 0$, respectively. It is then easy to see that

$$T_1 = T_K(J_1) \quad (17)$$

with $T_K(J)$ in Eq. (15), because all moments are decoupled for $T > T_1$. In contrast, T_2 has to be determined from

$$\frac{2}{J_2} = \int_{-\infty}^{+\infty} d\omega \frac{\rho_{c2}(\omega, T_2)}{\omega} \tanh\left(\frac{\omega}{2T_2}\right), \quad (18)$$

where $\rho_{c2}(\omega, T)$ is the *local* DOS of c electrons on sublattice B. While $\rho_{c2}(\omega)$ is simply given by $\rho_0(\omega + \mu)$ for $T > T_1$, the onset of Kondo screening on the A sublattice renormalizes ρ_{c2} in a temperature-dependent fashion, which is captured by the following equation:

$$\rho_{c2}(\omega, T) = \alpha(\omega, T) \rho_0(|\omega + \mu| \alpha(\omega, T)). \quad (19)$$

Here, $\alpha(\omega, T)$ is a “boost factor”, whose general form is given in appendix C. For $T > T_2$ it reduces to

$$\alpha(\omega, T) = \sqrt{\frac{-J_1 b_1(T)^2}{(\lambda_1(T) + \omega)(\mu(T) + \omega)}} + 1. \quad (20)$$

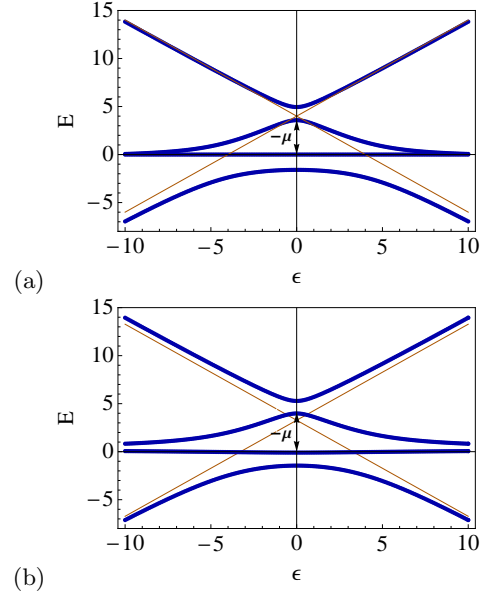


FIG. 3: Renormalized dispersions $E(\epsilon)$ (thick line) and bare dispersions (thin line) as a function of ϵ obtained from equation (11) for (a) $T_2 < T < T_1$ and (b) $T < T_2$. The bare c -electron DOS is constant, $\rho_0 = 1/(2D)$, with a half-bandwidth $D = 10$.

Due to the non-trivial temperature and frequency dependence of ρ_{c2} , the screening scale T_2 will not have the usual form (16) for the Kondo scale as a function of the Kondo coupling J_2 . Still, we expect that an increase of density of states at the Fermi level $\omega = 0$ to enhance this scale. We have, omitting the explicit temperature dependence of the mean-field parameters

$$\rho_{c2}(0) = \sqrt{\frac{-J_1 b_1^2}{\mu \lambda_1} + 1} \rho_0 \left(|\mu| \sqrt{\frac{-J_1 b_1^2}{\lambda_1 \mu} + 1} \right). \quad (21)$$

If $\rho_{c2}(0)/\rho_0(\mu) > 1$, the density of states at the Fermi level is enhanced by the first Kondo screening and we expect, accordingly, a boost of the B-sublattice Kondo screening, i.e., $T_2(J_2) > T_K(J_2)$. Alternatively, if $\rho_{c2}(0)/\rho_0(\mu) < 1$, the B-sublattice Kondo screening will be inhibited by the onset of the A-sublattice one. In general, the effect of $\alpha(\omega, T)$ is two-fold: as a factor affecting the argument of $\rho_0(\omega)$ (which may induce a particle-hole asymmetry) and as an overall coefficient. For a constant bare density of states, used for most of the numerical calculations, the first effect is absent. Otherwise, it will induce quantitative changes depending on the shape of ρ_0 – this happens, e.g., in the square-lattice case in Appendix B.

Before discussing numerical results for the screening scales $T_{1,2}$, it is enlightening to look at the renormalized dispersions $E(\epsilon)$ as obtained from Eq. (11) by solving the set of mean-field equations. Fig. 3 displays the generic resulting bands for $T_2 < T < T_1$ and $T < T_2 < T_1$. For temperatures $T_2 < T < T_1$ (Fig. 3a), the local moments

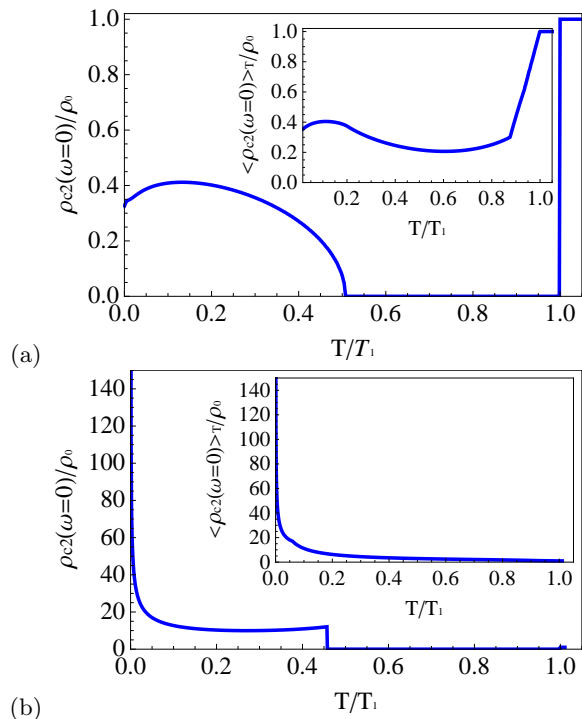


FIG. 4: Temperature evolution of the normalized density of states at the Fermi level $\rho_{c2}(0)/\rho_0(\mu)$ (see Eq. (21)) of c electrons in the second sublattice for $J_2 = 0$ at an electronic filling number (a) $n_c = 0.2$, (b) $n_c = 0.9$. The temperature scale is normalized by T_1 , the first Kondo coupling is $J_1 = 8$ and the half-bandwidth is set to $D = 10$. The bare density of states ρ_0 is taken constant in its support. Inset: averaged normalized density of states $\langle \rho_{c2}(0) \rangle_T / \rho_0(\mu)$ in a window of width $\sim T$ around the Fermi level.

of the B sublattice are unscreened; in the mean-field approach, this is signaled by a flat band being located at the Fermi level $\omega = 0$. Hence, three renormalized bands form, one of which is narrow and primarily of f character. If only nearest-neighbor hopping is considered, the symmetry of the DOS imposes that at half-filling, $n_c = 1$ at $\mu = 0$, this narrow band is completely flat and located at $\omega = 0$. Away from half-filling, the width of this narrow band is then linear in $|\mu|$. With an asymmetric DOS, the width of the narrow band still reaches its minimum at half-filling (but does not vanish). The dependence of this width on the chemical potential μ indicates a strong effect of the conduction-band filling n_c on the B-sublattice Kondo screening. Lowering the temperature further below T_2 (Fig. 3b), a hybridization gap opens near the Fermi level, and the second f -level transforms into a weakly dispersive heavy band crossing the Fermi level.

B. Competitive vs. co-operative Kondo screening

We are now in the position to discuss whether the Kondo effects on the two sublattices compete or co-

operate. To quantify this effect, we shall compare the screening-onset temperature T_2 of the B-sublattice moments in our model with Kondo couplings $J_1 > J_2$ to the screening-onset temperature of a homogeneous Kondo lattice with the same bare DOS where all Kondo couplings are set to J_2 – the latter temperature is simply given by $T_K(J_2)$ according to Eq. (15).

As T_2 is determined by Eq. (18), we first focus on the relevant B-sublattice local DOS $\rho_{c2}(\omega, T)$. Fig. 4 shows the temperature evolution of the normalized DOS at the Fermi level $\rho_{c2}(\omega = 0)/\rho_0(\mu)$ for different values of the electronic filling $n_c = 0.2$ and 0.9 . Note that we have formally set $J_2 = 0$, such that all temperatures obey $T > T_2$. For both cases, $\rho_{c2}(0)$ vanishes in an intermediate-temperature regime below T_1 , as none of the quasiparticle bands crosses the Fermi level. The system is still metallic: the averaged density of states in a window of width $\sim T$ around the Fermi level is finite, see the insets of Fig. 4. At very low temperatures, we recover a finite density of states $\rho_{c2}(0)$, as we expect for a metallic state, except at quarter filling, $n_c = 0.5$, where $\rho_{c2}(0) = 0$ at all temperatures below T_1 and a band insulator is obtained. This can be understood using a counting argument: at quarter-filling, and for $J_2 = 0$, the large Fermi surface encompasses an even number $2n_c + 1 = 2$ of particles and a band gap at the Fermi level is expected.

The crucial difference between Figs. 4a and 4b is that for $n_c = 0.2$, and generically below quarter-filling, $\rho_{c2}(0)$ is smaller than $\rho_0(\mu)$ at low temperature. Accordingly, we expect the B-sublattice Kondo effect to be reduced as compared to the homogeneous case. In contrast, for $n_c = 0.9$, and generically above quarter-filling, $\rho_{c2}(0)$ is strongly enhanced. This enhancement reaches its maximum at half-filling where the width of the narrow band reaches its minimal value as discussed earlier. Accordingly, we expect a sensitive boost of the second Kondo effect when $J_2 \ll J_1$. At quarter-filling, because the density of states at the Fermi level vanishes at all temperatures below T_1 , a second Kondo screening occurs only above a finite critical value J_{2c} .

The B-sublattice screening scale T_2 , as obtained from Eq. (18), is displayed in Fig. 5 for different values of the conduction-band filling n_c . At all fillings, the strength of the second Kondo scale is consistent with the expectations drawn from Fig. 4 for $J_2 \ll J_1$: a reduction (enhancement) of the B-sublattice c -electron local DOS results in a suppression (promotion) of the B-sublattice Kondo effect.

When $n_c \ll 1/2$, the second Kondo effect is inhibited for all values of $J_2 < J_1$ (Fig. 5a), whereas it is promoted for $1/2 \ll n_c < 1$ for all values of $J_2 < J_1$ (Fig. 5c). It is worth emphasizing that the suppression of T_2 for small n_c is a drastic effect: Even small differences between J_1 and J_2 can induce largely different T_1 and T_2 , Fig. 5a. Close to quarter-filling, a crossover regime is found for which the B-sublattice Kondo effect is promoted for $J_2 \ll J_1$ and inhibited for intermediate values of J_2 up to J_1 (Fig. 5b). For these intermediate

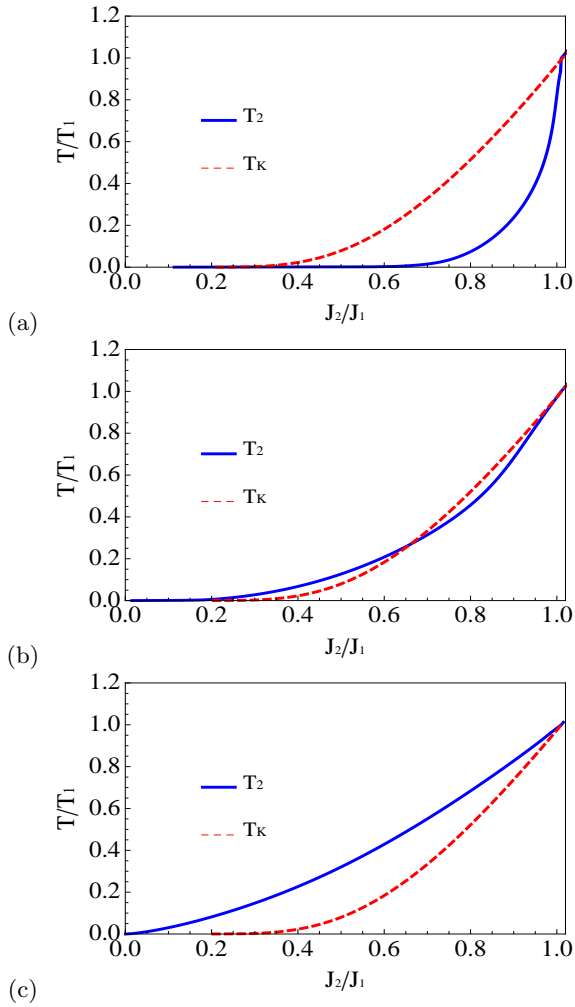


FIG. 5: Evolution of the temperature scales $T_2(J_2), T_K(J_2)$, where $T_K(J_2)$ is the Kondo scale obtained in the homogeneous Kondo lattice with a Kondo coupling J_2 , with the strength of the second coupling constant $J_2 \leq J_1$ for an electronic filling number: a) $n_c = 0.2$, (b) $n_c = 0.6$ and (c) $n_c = 0.9$. The temperature scale is normalized by T_1 , and the one of J_2 by J_1 . The bare density of states ρ_0 used is constant in its support.

values of J_2 , it is not straightforward to deduce the effect of the A-sublattice Kondo effect on the B-sublattice one because the density of states at the Fermi level $\rho_{c2}(0)$ is vanishing in an intermediate energy regime. One has then to consider the full integral in (18) instead of focusing on its usually dominant $\omega = 0$ contribution. We found this transition regime to depend on the shape of the bare DOS.

C. Kondo feedback

So far, we have considered the effect of the A-sublattice Kondo screening on the B-sublattice one, mainly in the extreme inhomogeneous case of small J_2 . We now discuss

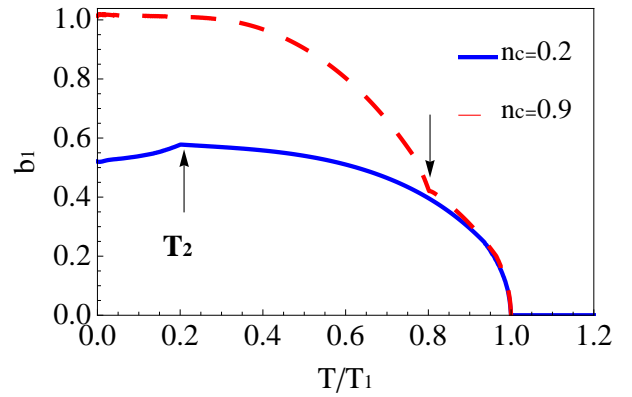


FIG. 6: Temperature dependence of the A-sublattice condensate b_1 for $J_2 = 7, J_1 = 8$ at different filling numbers $n_c = 0.2, 0.9$. The temperature scale is normalized by T_1 . The arrows point to the kinks occurring at the second Kondo scale T_2 . The bare density of states ρ_0 used is constant in its support with a half-bandwidth $D = 10$.

the “feedback” effect of the B-sublattice screening on the A-sublattice one. We have already emphasized that the A-sublattice Kondo scale is the same as the one obtained for the homogeneous case $J_1 = J_2$. That is because this scale depends on the bare density of states of c electrons. Fig. 6 shows the generic temperature evolution of the A-sublattice condensate b_1 at two different filling numbers n_c . A kink is observed as soon as the B-sublattice Kondo effect sets in. Below quarter-filling, when an inhibition of the B-sublattice Kondo screening is observed, b_1 is reduced below T_2 , whereas it increases above quarter-filling, saturating at low temperatures. This means that the two Kondo effects are either mutually co-operative (above quarter filling) or mutually competitive (below quarter filling). Fig. 7 shows the generic temperature evolution of the average occupation number n_{c1} in the

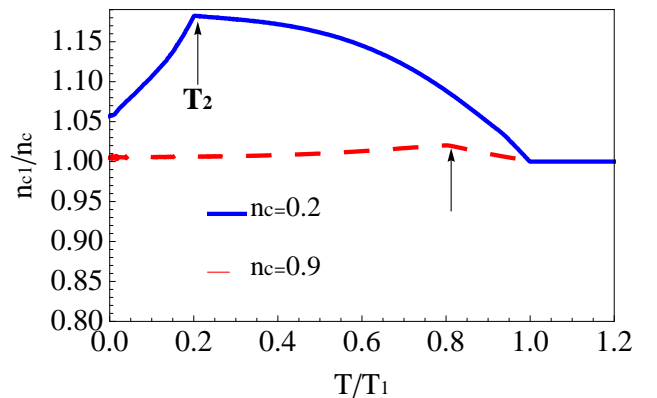


FIG. 7: Temperature evolution of the average occupation number n_{c1} in the first sublattice for $J_2 = 7, J_1 = 8$ at different filling numbers $n_c = 0.2, 0.9$. The temperature scale is normalized by T_1 and n_{c1} is normalized by the total filling number n_c . The arrows point to the kinks occurring at the second Kondo scale T_2 . The bare density of states ρ_0 used is constant in its support with a half-bandwidth $D = 10$.

A sublattice at two different fillings $n_c = 0.2, 0.9$. It turns out that for all fillings n_c this quantity increases as soon as the A-sublattice Kondo effect sets in, i.e. there are more electrons on the A sublattice as compared to B (recall that, for $T > T_1$, both fillings are equal in our model). At the onset of the B-sublattice Kondo effect, n_{c1} reduces again without necessarily recovering its high-temperature value.

The fact that n_{c1} increases for all values of filling number n_c as soon as the A-sublattice Kondo effect sets in means that the latter sustains itself not only by involving low energy, i.e. near the Fermi energy, conduction electrons in the second sublattice but also *high energy* ones. It shows also that the average number of c electrons in the B sublattice n_{c2} plays little role, compared to the density of states ρ_{c2} , in identifying a promotion or inhibition regime for the second Kondo effect.

IV. LOW-TEMPERATURE PROPERTIES OF THE FERMI-LIQUID STATE

At sufficiently low temperatures, we expect our model system to behave as a Fermi liquid (neglecting possible magnetic or superconducting instabilities and provided that no Kondo insulator obtains). The Fermi liquid can be characterized by its linear-in-temperature specific heat $C(T)/T \approx \gamma$, constant magnetic susceptibility χ_0 and quadratic-in-temperature resistivity $\rho(T) - \rho_0 \approx AT^2$. This Fermi-liquid behavior will be realized below a so-called coherence scale T_{coh} , which governs the low-temperature properties of thermodynamic and transport quantities and takes the role of an effective Fermi energy of the heavy quasiparticles.

For the case of a homogeneous Kondo lattice, studies using local self-energy approximations to the Kondo lattice model (i.e. dynamical mean-field theory and slave bosons) have shown that is different from T_K , but shares its exponential dependence on the Kondo coupling J .^{20–22,30} In particular, their ratio has been found to be independent of J . In this section, we explore this issue in the case of two inequivalent local moments per unit cell. The effective four-band picture is particularly appropriate to describe the Fermi-liquid regime that sets in at very low temperatures.

In the low-temperature limit, thermodynamic quantities, such as the electronic entropy $S_e(T)$ or the electronic specific heat coefficient $C(T)$, are determined by the density of states at the Fermi level $\rho(0)$

$$S_e(T \rightarrow 0) = \frac{\pi^2}{6} \rho(0) T, \quad C(T \rightarrow 0) = \frac{\pi^2}{6} \rho(0) T. \quad (22)$$

Following Ref. 20, one may define a coherence scale in terms of the zero-temperature value of the average renormalized density of electronic states at the Fermi level $\rho(0) = \frac{1}{2} \sum_{\nu} (\rho_{c\nu}(0) + \rho_{f\nu}(0))$ as follows (recall

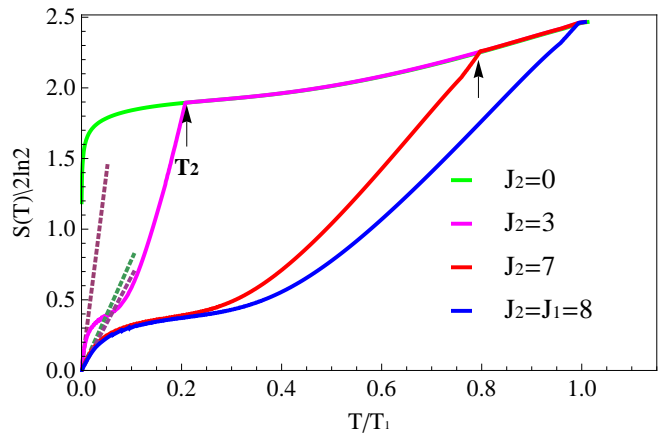


FIG. 8: Total average entropy, normalized by $2 \ln 2$,³² at filling number $n_c = 0.9$ for different values of $J_2 = 0, 3, 7$ and $J_1 = 8$. The temperature scale is normalized by T_1 . Tiny dashed lines are linear fit at very low temperatures. The arrows point to the kinks occurring at the second Kondo scale T_2 . The bare density of states ρ_0 used is constant in its support with a half-bandwidth $D = 10$.

$$k_B = 1)^{31}$$

$$\bar{T}_{\text{coh}} \equiv \frac{1}{4\rho(0, T=0)} \quad (23)$$

so that the low-temperature expansion of thermodynamic and transport quantities may be written in terms of powers of T/\bar{T}_{coh} . The same applies to our mean-field parameters which are expected to saturate to their zero-temperature value sufficiently below \bar{T}_{coh} . As \bar{T}_{coh} is, strictly speaking, a scale characterizing the $T = 0$ state only, we define $T_{\text{coh}} = \min\{\bar{T}_{\text{coh}}, T_1, T_2\}$. (Note that $\bar{T}_{\text{coh}} < T_2$ except in the proximity to Kondo-insulating states.)

A. Entropy

Fig. 8 shows the temperature dependence of the total average entropy for different coupling constants J_2 above quarter-filling, here $n_c = 0.9$.

We first discuss the extremely inhomogeneous case $J_2 = 0$, corresponding to decoupled B -sublattice moments. Here, the entropy starts to drop slowly below T_1 , remaining close to $4 \ln 2$, then decreases steeply towards low temperature to reach $2 \ln 2$ at $T = 0$. This residual entropy corresponds to the one of the unscreened local moments in the second sublattice.³² Once this contribution is subtracted, a linear dependence is found at low temperature consistent with the formation of a coherent Fermi liquid state, involving conduction electrons in both sublattices as well as the screened local moments on the A sublattice (while the B local moments are decoupled), with a finite “coherence” scale T_{coh} .

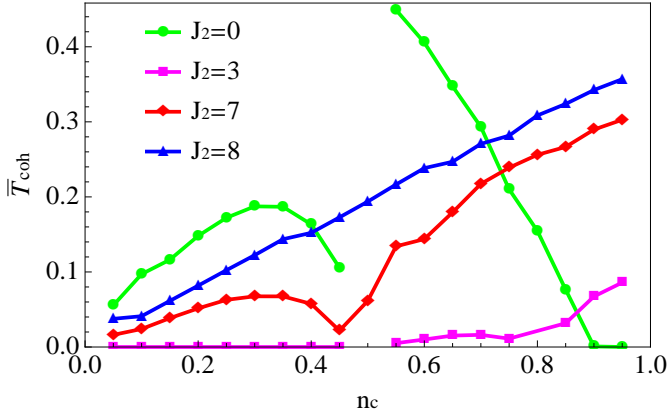


FIG. 9: Evolution of the coherence scale \bar{T}_{coh} with the electronic filling n_c for different values of the coupling constant $J_2/J_1 = 0, 3/8, 7/8, 1$. The bare density of states ρ_0 used is constant in its support with a half-bandwidth $D = 10$.

For finite values of J_2 , a second kink signals the onset of the second Kondo screening at T_2 . Then a stronger decrease is observed in the entropy below this scale. This decrease can be followed by a plateau-like feature close to half filling. (This feature is absent below quarter-filling.) At lower temperatures, the entropy is again linear in temperature signaling the emergence of a Fermi liquid regime out of the conduction electrons and the local moments in both sublattices.

B. Coherence scale

Fig. 9 shows the evolution of the coherence scale \bar{T}_{coh} with the filling number for different values of J_2 . In all cases, \bar{T}_{coh} approaches zero as $n_c \rightarrow 0$ as a result of “exhaustion”.¹⁹

Again, we start with the extremely inhomogeneous case $J_2 = 0$. Here, a band insulator is obtained at quarter-filling and T_{coh} is not defined. Above quarter-filling, the coherence scale for $J_2 = 0$ decreases down to zero at half-filling. This can be understood by looking at the renormalized band structure (see Fig. 3). The width of the band crossing the Fermi level is of order μ , the chemical potential. As we increase the filling number n_c towards half-filling, this quantity, proportional to \bar{T}_{coh} , decreases towards zero. The argument for \bar{T}_{coh} going to zero at half-filling relies on the fact that the bare DOS is symmetric, and thus that $\mu = 0$ at half-filling. However, we observed that the decrease of \bar{T}_{coh} above quarter-filling holds even with the inclusion of next-nearest neighbor hopping, i.e. for a asymmetric bare DOS, albeit not towards zero at half-filling.

For finite J_2 , the behavior of \bar{T}_{coh} is consistent with the observations regarding the promotion or inhibition of the B-sublattice Kondo effect, as its scale T_2 sets an upper bound on \bar{T}_{coh} . This is more easily seen in Fig. 10, where we compare \bar{T}_{coh} to the homogeneous case’s result. At

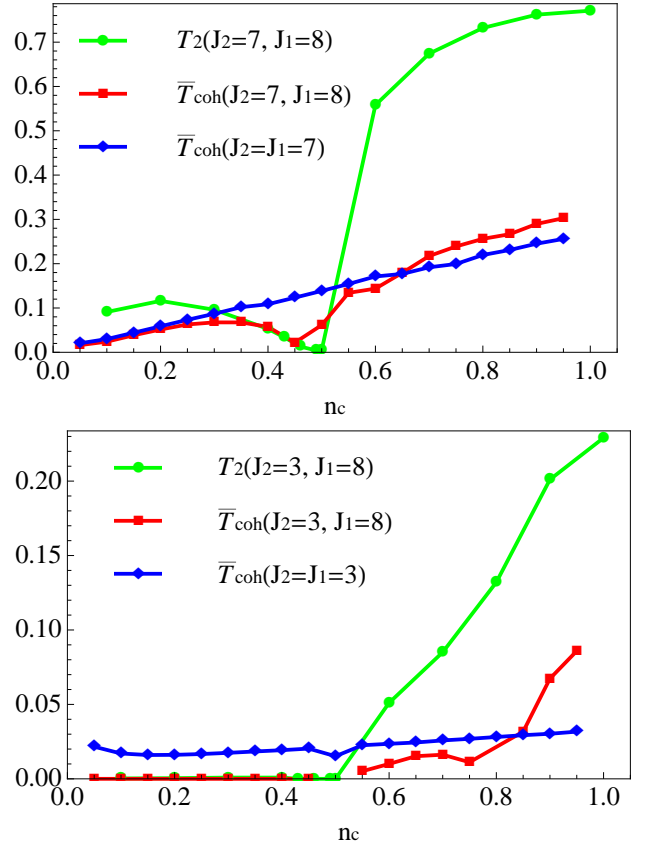


FIG. 10: Evolution of the coherence scale \bar{T}_{coh} and the second Kondo scale T_2 with the electronic filling n_c for coupling constants $J_2/J_1 = 7/8$ (upper panel) and $J_2/J_1 = 3/8$ (lower panel). Also shown is \bar{T}_{coh} for the homogeneous case $J_1 = J_2$. The bare density of states ρ_0 used is constant in its support with a half-bandwidth $D = 10$.

low fillings, the coherence scale \bar{T}_{coh} is smaller compared to the homogeneous case, consistent with the inhibition of the second Kondo effect: the mean-field parameters saturate at lower temperatures compared to the homogeneous case. The opposite happens above, where \bar{T}_{coh} is increased, consistent with the promotion of the second Kondo effect. Its effect on \bar{T}_{coh} is most pronounced close to half filling.

It is worth discussing the contributions to the total DOS $\rho(0)$, which defines our \bar{T}_{coh} . Consider the ratio between the densities of states of the two sublattices:

$$\begin{aligned} \frac{\rho_1(0)}{\rho_2(0)} &\equiv \frac{(1 + \frac{J_1 b_1^2}{\lambda_1^2}) \rho_{c1}(0)}{(1 + \frac{J_2 b_2^2}{\lambda_2^2}) \rho_{c2}(0)} \\ &= \frac{1}{\alpha(0)^2} \frac{(1 + \frac{J_1 b_1^2}{\lambda_1^2})}{(1 + \frac{J_2 b_2^2}{\lambda_2^2})}, \end{aligned} \quad (24)$$

where $\alpha(0)$ is the boost factor given by

$$\alpha(0) = \sqrt{\frac{1 - \frac{J_1 b_1^2}{\lambda_1 \mu}}{1 - \frac{J_2 b_2^2}{\lambda_2 \mu}}},$$

see Eq. (C2) in Appendix C for details. The ratio (24) is mainly controlled by two quantities: the boost factor α and the relative contributions coming from the heavy f -like bands forming below the Kondo scales.

Fig. (11) shows the contributions of each sublattice to the total DOS $\rho(0) = 1/(4\bar{T}_{\text{coh}})$ for different electronic fillings n_c and couplings J_2 . For $0 < J_2/J_1 \ll 1$, the total DOS is dominated mainly by contributions from the B sublattice for the lowest electronic filling up to $n_c \sim 0.75$ then decreases below the contribution from the A sublattice before converging to one half towards half filling. In this regime of Kondo couplings, and for low electronic filling, the main contribution comes from the f -like heavy band formed out of local moments in the B sublattice (regardless of the small boost factor). We note that the detailed behavior near $n_c \sim 0.8$ depends on the input c -electron DOS and is different for the square-lattice case.

For $J_2/J_1 \lesssim 1$, contributions from the A sublattice dominates for very low electronic fillings before being over passed by the contribution from the B sublattice already below quarter filling. The latter contribution attains its relative maximum at quarter filling before reducing towards one half, both contributions being equal at half filling. Here the effect of the boost factor wins over the effect originating from the two f -like heavy bands and mainly sets the behavior of the ratio (24)

An interesting feature for the different investigated shapes of DOS and $0 < J_2/J_1$ ratios, when only nearest-neighbor hopping is considered, is the convergence towards equal contributions from each sublattice when approaching half filling, $n_c \rightarrow 1$. This is due to the symmetry of the DOS that imposes $\mu = 0$ at half-filling. In this case, one can check from (24) that $\mu \rightarrow 0$ causes $\rho_1(0)/\rho_2(0) \rightarrow 1$ for all values of J_2 and J_1 .

V. DISCUSSION

A. Summary

In this paper, we have investigated the interplay between two sublattice Kondo effects in a bi-partite Kondo lattice model with two spin-1/2 local moments per unit cell, with Kondo couplings $J_1 > J_2$ on sublattices A,B. We have found that the conduction-band filling n_c determines how the B-sublattice Kondo effect is affected by the onset of A-sublattice Kondo screening: it is generically promoted for $n_c > 0.5$ and inhibited for $n_c < 0.5$. Our collected results thus show that quarter filling, $n_c = 0.5$, is the boundary separating regimes where the two Kondo

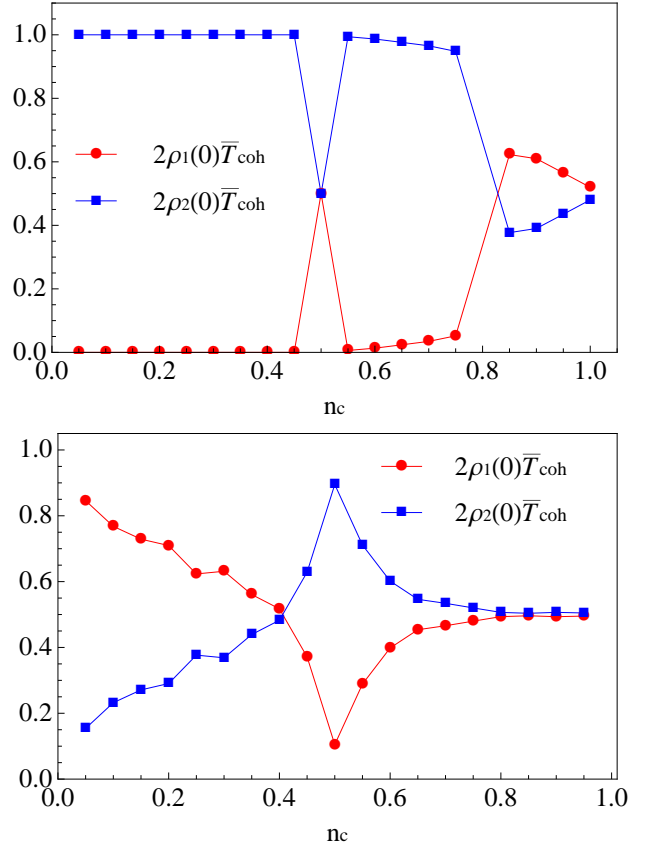


FIG. 11: Contributions of each sublattice to the low-temperature average density of states at the Fermi level $\rho(0) = 1/4\bar{T}_{\text{coh}}$, illustrated for different electronic filling n_c and $J_2/J_1 = 3/8$ (top) and $J_2/J_1 = 7/8$ (bottom). $\rho_\nu \equiv \rho_{c\nu} + \rho_{f\nu}$ is the density of states of sublattice ν . The bare density of states ρ_0 used is constant in its support.

effects are either mutually co-operative ($n_c > 1/2$) or mutually competitive ($n_c < 1/2$). A strong competition in the latter regime implies that *small* differences between J_1 and J_2 induce *large* differences between T_1 and T_2 as a result of non-trivial feedback effects, see Fig. 5a. Therefore, the regime of partial screening advocated in the introduction may be reached easily for small conduction band filling.

B. Relation to depleted Kondo lattices

Heavy fermion systems with randomly depleted local moments constitute an interesting route to interpolate between the physics of isolated Kondo impurities and coherent Kondo lattice behavior. Experimentally, depletion is realized by substituting magnetic by non-magnetic ions, as e.g. in $\text{Ce}_{1-x}\text{La}_x\text{Al}_3$. Theoretically, a number of papers have treated depleted Kondo lattices,^{25–27} with randomly distributed local moments with concentration $n_f < 1$, mainly using local self-energy approximations, combined either with CPA or with a numerically exact

treatment of spatial disorder. One of the remarkable findings is that $n_f = n_c$ marks a boundary between two distinct regimes: For $n_f < n_c$ the behavior is akin to that of dilute impurities, i.e., lattice effects appear to be small, whereas $n_f > n_c$ leads to Kondo lattice behavior. Although both regimes are Fermi-liquid-like at lowest temperatures, the crossover is rather pronounced e.g. in the coherence temperature $T_{\text{coh}}(n_f)$ which is approximately constant for $n_f < n_c$, but rapidly drops upon increasing n_f beyond n_c . The latter behavior may be related to “exhaustion”, i.e., the lack of conduction electrons to screen the moments. It has been speculated that the boundary $n_f = n_c$ is inherited from the strong-coupling limit, $J \rightarrow \infty$, where $n_f = n_c$ represents a (random) Kondo insulator.²⁵

We believe that the two seemingly different problems of depleted Kondo lattices and Kondo lattices with inequivalent local moments are related in the following way: For $T_2 < T < T_1$ in the latter problem, Kondo screening is “active” for half of the moments. This can be read as an $n_f = 1/2$ depleted Kondo lattice, albeit without randomness. Carrying over the results of Refs. 25–27 suggests that $n_c < 1/2$ then corresponds to a collective regime with exhaustion playing a role. As a result, conduction electrons are strongly involved in screening A-sublattice moments, such that B-sublattice screening is suppressed and the two Kondo effects compete. In contrast, for $n_c > 1/2$ a single-ion picture is more appropriate: Kondo screening of A sites injects states near the Fermi level, such that B-sublattice screening is promoted and the two Kondo effects co-operate. These arguments, although somewhat simplistic, are consistent with our numerical results for ρ_{c2} in Sec. III B.

C. Extensions

A natural extension of the calculations presented here is to take into account non-local magnetic correlations, due to either RKKY interactions or a direct Heisenberg-like exchange. In addition to the standard Kondo lattice phenomenology, i.e., the occurrence of magnetic (or spin-liquid) phases for dominant inter-moment exchange, interesting physics can be expected in the regime of partial screening, see Fig. 1. For instance, for small J_2 the B-sublattice moments are more susceptible to non-local effects than the A-sublattice moments, paving the way to either non-local B-sublattice “screening” or B-sublattice-dominated magnetic order.

One might also speculate about variants of the Kondo-breakdown (KB) scenario for quantum criticality, originally proposed as a possible description of some fascinating non-Fermi liquid properties in heavy fermion systems.^{33–35} A central role in this scenario is played by so-called fractionalized Fermi-liquid states, formed out of conduction electrons weakly coupled to an exotic (i.e. fractionalized) spin liquid.³⁴ In the present situation with two local moments per unit cell, a “conventional” spin liq-

uid with intra-cell dimer formation are possible, leading to a light metallic state with Fermi-liquid properties, similar to that in the bilayer Kondo lattice model of Ref. 36. However, exotic spin liquids may be formed e.g. from the B-sublattice moments only, such that a fractionalized Fermi liquid may be realized in the regime of partial screening. A comprehensive study of these issues is left for future work.

D. Experiments

At present, relatively little detailed information is available about the low-temperature properties of the $(\text{RE})_3\text{Pd}_{20}\text{X}_6$ compounds mentioned in the introduction. Clearly, a detailed characterization of the ordered phases, e.g., by neutron scattering, is desirable to put those in the global perspective advocated here.

Based on our results, we propose to perform systematic doping studies of these compounds, using dopants of different valence. As shown here, variations in the conduction electron filling can be expected to significantly affect the different Kondo scales in the system.

Acknowledgments

We thank A. Hackl, A. Mitchell, A. Rosch, and E. Sela for fruitful discussions. This research was supported by the DFG through SFB 608 and FOR 960.

Appendix A: Review of slave-boson results for the standard Kondo lattice

Here, we recall some results from the mean-field approximation of the Kondo lattice problem. An extensive presentation can be found in Ref. 30.

The mean-field equations are written as follows

$$\begin{aligned} b &= \sqrt{J} \int_{-\infty}^{\infty} d\omega \rho_{fc}(\omega) n_F(\omega), \\ 1 &= 2 \int_{-\infty}^{\infty} d\omega \rho_f(\omega) n_F(\omega), \\ n_c &= 2 \int_{-\infty}^{\infty} d\omega \rho_c(\omega) n_F(\omega), \end{aligned} \quad (\text{A1})$$

where $n_F(\omega)$ is the Fermi function and $\rho_c, \rho_f, \rho_{fc}$ are the spectral densities of the local single-particle Green’s functions given as

$$\begin{aligned} \rho_c(\omega) &\equiv -\frac{1}{\pi} \Im \mathcal{G}_{cc}^+(\omega) = \rho_0(\epsilon(\omega)), \\ \rho_{fc}(\omega) &\equiv -\frac{1}{\pi} \Im \mathcal{G}_{fc}^+(\omega) = \frac{\sqrt{J}b}{\omega + \lambda} \rho_c(\omega), \\ \rho_f(\omega) &\equiv -\frac{1}{\pi} \Im \mathcal{G}_{ff}^+(\omega) = \frac{Jb^2}{(\omega + \lambda)^2} \rho_c(\omega), \end{aligned} \quad (\text{A2})$$

where $\mathcal{G}^+(\omega) \equiv \mathcal{G}(i\omega \rightarrow \omega + i0^+)$ is the retarded Green's function matrix and $\epsilon(\omega) = \omega + \mu - \frac{Jb^2}{\omega + \lambda}$.

Notice that

$$(n_c + 1) \bmod 2 = \int_{-\infty}^{\mu_L} \rho_0(\omega), \quad (\text{A3})$$

where $\mu_L \equiv \mu - \frac{Jb^2}{\lambda}$ can be understood as a chemical potential corresponding to the enlarged Fermi volume, which encompasses $n = n_c + 1$ electrons when $b \neq 0$.

The Kondo temperature T_K is defined as the temperature for which the effective hybridization $\propto b$ vanishes. It is obtained from the mean-field equations (A2) in the limit $b, \lambda \rightarrow 0$. This gives

$$\frac{2}{J} = \int_{-\infty}^{+\infty} d\omega \frac{\rho_0(\omega + \mu)}{\omega} \tanh\left(\frac{\omega}{2T_K}\right). \quad (\text{A4})$$

For $\rho_0(\mu) \neq 0$, the main contribution to the integral in (A4) comes from $\omega = 0$ and any finite coupling J leads to $T_K > 0$. In the weak coupling regime $J \ll D$, one finds²⁰

$$T_K = \alpha_0 \sqrt{D^2 - \mu^2} F_K e^{-1/J\rho_0(\mu)}, \quad (\text{A5})$$

where $\alpha_0 = 1.13$ is a numerical constant and

$$F_K = \exp \left[\int_{-(D+\mu)}^{D-\mu} d\omega \frac{\rho_0(\omega + \mu) - \rho_0(\mu)}{2|\omega|\rho_0(\mu)} \right] \quad (\text{A6})$$

In the Kondo lattice problem, the Kondo scale T_K is not necessarily the one that characterizes the behavior of the low-temperature regime. Generally, the thermodynamic quantities like the specific heat coefficient or the zero temperature magnetic susceptibility are characterized by a second energy scale given by³⁰

$$\bar{T}_{\text{coh}} = \frac{D + \mu}{\Delta\mu} \frac{F_0}{\rho_0\mu} e^{-1/J\rho_0(\mu)}, \quad (\text{A7})$$

where $\Delta\mu = \mu_L - \mu$ and

$$F_0 = \exp \left[\int_{-(D+\mu)}^{\Delta\mu} d\omega \frac{\rho_0(\omega + \mu) - \rho_0(\mu)}{|\omega|\rho_0(\mu)} \right]. \quad (\text{A8})$$

From (A5) and (A7), we see that the scales T_K and \bar{T}_{coh} have the same exponential dependence on the coupling constant J . They can differ considerably in their prefactors. Their ratio depends generally on the electronic filling and the shape of the density of states. Well below $T_{\text{coh}} = \min\{\bar{T}_{\text{coh}}, T_K\}$, the system behaves as a Fermi liquid for less than half-filling.

Appendix B: Results for the inhomogeneous square lattice

In this appendix, we present some results for the Kondo lattice problem with two inequivalent local moments, Eq. (1), on a square lattice of c -electron orbitals.

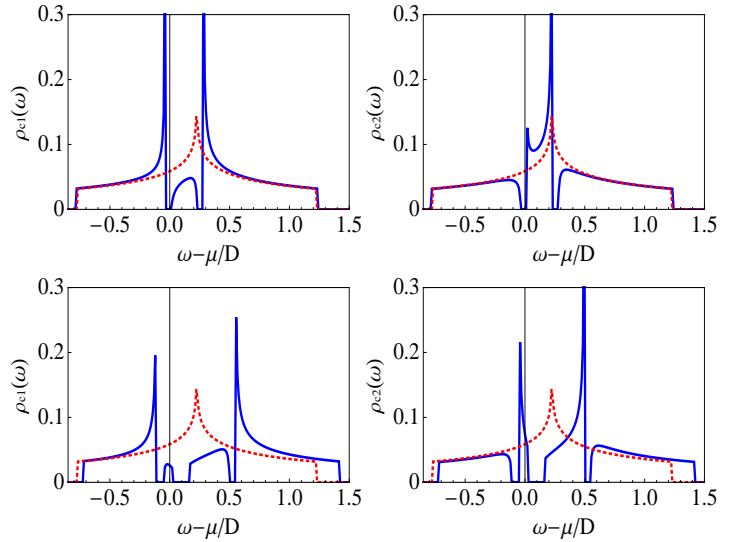


FIG. 12: Densities of states of the c -electrons in each sublattice, left for sublattice A and right for B, for $T_2 < T < T_1$ (top panels) and $T < T_2$ (bottom panels) in the square lattice case with no next-nearest neighbor hopping. The bare density of states for $T > T_1$ is shown in dashed line in each panel. The half bandwidth is $D = 10$.

Restricting ourselves first to the case of nearest-neighbor hopping only, we can apply the numerical machinery as in the body of the paper, i.e., the momentum summations can be converted into frequency integrals. To this end, one needs the c -electron density of states, which is given by

$$\rho_{\square}(\omega) = \frac{2}{\pi^2 D} \mathcal{K} \left(\sqrt{1 - \frac{\omega}{D}} \right) \theta(D^2 - \omega^2), \quad (\text{B1})$$

where $\mathcal{K}(x)$ is the elliptic integral of the first kind, and $D = 4t$ where t is the nearest-neighbor hopping. This DOS is smooth and continuous, except at the step-like

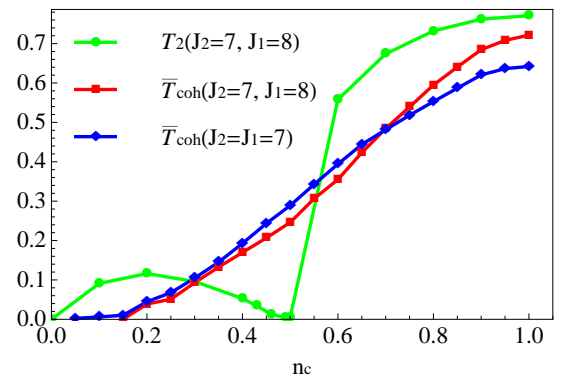


FIG. 13: Evolution of the coherence scale \bar{T}_{coh} and the Kondo scale T_2 with the electronic filling n_c for a coupling constant $J_2/J_1 = 7/8$ and comparison with the standard Kondo lattice result for the square lattice case with no next-nearest neighbor hopping. The half bandwidth is $D = 10$.

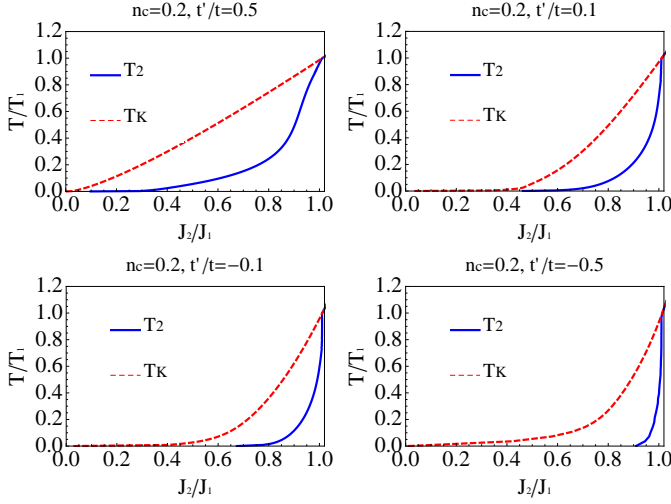


FIG. 14: Evolution of the temperature scales $T_2(J_2)$ and $T_K(J_2)$, where $T_K(J_2)$ is the Kondo scale obtained in the homogeneous Kondo lattice with a Kondo coupling J_2 , with the strength of the second Kondo coupling $J_2 \leq J_1$ for an electronic filling $n_c = 0.2$ and various values of the next-nearest hopping parameter t' .

band edges and at the $\omega = 0$ van Hove singularity, where the DOS diverges as $\rho_{\square}(\omega) \sim \frac{2}{\pi^2 D} \log \frac{4D}{|\omega|}$.

Fig. 12 shows the temperature evolution of the local DOS for the c electrons in each sublattice for the square lattice with no next-nearest neighbor hopping. This evolution is consistent with Fig. 3 showing the renormalized dispersions at $T_2 < T < T_1$ and $T < T_2$.

Fig. 13 shows the dependence of the coherence and Kondo scales on the electronic filling number n_c for $J_2 \simeq J_1$ and $J_2 = J_1$ and how they compare to the coherence scale in the homogeneous case. This is qualitatively similar to Fig. 9: for low fillings, the coherence scale \bar{T}_{coh} is smaller compared to the homogeneous Kondo lattice case then bigger above quarter filling, when we approach half filling. Thus, the qualitative picture developed in the body of the paper is reproduced for the square lattice.

Finally, we investigate the effect of the inclusion of next-nearest hopping, with a parameter t' . Non-zero t' results in non-vanishing momentum-dependent diagonal terms $\xi_{\mathbf{k}} = \zeta_{\mathbf{k}} = -4t' \cos(k_x) \cos(k_y)$ in the kinetic matrix $\mathcal{E}_{\mathbf{k}}$ in (6). Then, momentum summations in the mean-field equations (9) can no longer be turned into an integration over energies. Instead, the mean-field equations are now solved on a discrete lattice of 64^2 sites.

Figs. 14 and 15 show the dependence of the B-sublattice Kondo scale and the Kondo scale in the homogeneous case on the electronic filling n_c for various values of the next-nearest hopping parameter t' .

Our conclusion on the promotion or the inhibition of the second Kondo effect is found to be robust against inclusion of next-nearest neighbor hopping, namely inhibition below quarter-filling and promotion above quarter-filling.

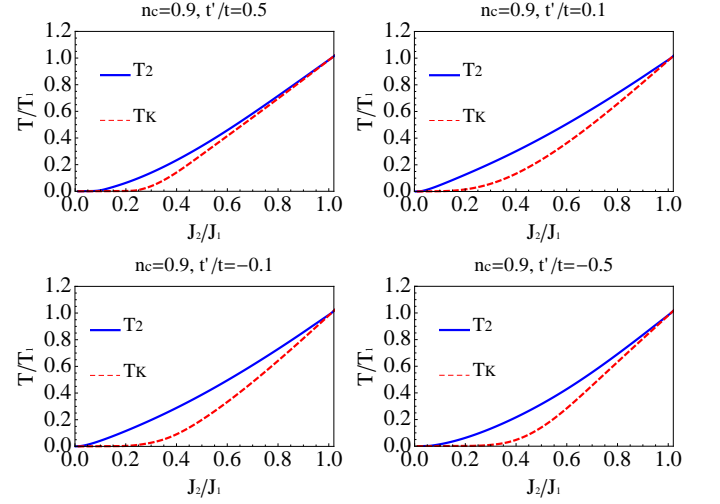


FIG. 15: Evolution of the temperature scales $T_2(J_2)$ and $T_K(J_2)$, where $T_K(J_2)$ is the Kondo scale obtained in the homogeneous Kondo lattice with a Kondo coupling J_2 , with the strength of the second Kondo coupling $J_2 \leq J_1$ for an electronic filling $n_c = 0.9$ and various values of the next-nearest hopping parameter t' .

Appendix C: Spectral densities

The mean-field equations (9) can be written alternatively using the spectral densities of the local single-particle Green's functions

$$\begin{aligned} b_{\nu} &= \sqrt{J_{\nu}} \int_{-\infty}^{\infty} d\omega \rho_{fc\nu}(\omega) n_F(\omega), \\ 1 &= 2 \int_{-\infty}^{\infty} d\omega \rho_{f\nu}(\omega) n_F(\omega), \\ n_{c\nu} &= 2 \int_{-\infty}^{\infty} d\omega \rho_{c\nu}(\omega) n_F(\omega), \end{aligned} \quad (\text{C1})$$

where $n_F(\omega) = 1/(1 + e^{\omega/T})$ is the Fermi function. If we consider only nearest-neighbor hopping, we can have analytic expressions for the spectral densities $\rho_{c\nu}, \rho_{f\nu}, \rho_{fc\nu}$

$$\begin{aligned} \rho_{c\nu}(\omega) &= \alpha^{\nu}(\omega) \rho_0(\epsilon(\omega)), \\ \rho_{f\nu}(\omega) &= \frac{J_{\nu} b_{\nu}^2}{(\omega + \lambda_{\nu})^2} \rho_{c\nu}(\omega), \\ \rho_{fc}^{\nu}(\omega) &= \frac{\sqrt{J_{\nu}} b_{\nu}}{\omega + \lambda_{\nu}} \rho_{c\nu}(\omega), \end{aligned} \quad (\text{C2})$$

where

$$\alpha^{\nu}(\omega) = \sum_{\beta} \Lambda_{\nu\beta} \sqrt{\frac{(\lambda_{\nu} + \omega)(J_{\beta} b_{\beta}^2 - (\lambda_{\beta} + \omega)(\mu + \omega))}{(\lambda_{\beta} + \omega)(J_{\nu} b_{\nu}^2 - (\lambda_{\nu} + \omega)(\mu + \omega))}},$$

defines the boost factor and $\epsilon(\omega)$ is given in Eq. (12). Here $\Lambda_{\nu\beta}$ are matrix elements of the 2×2 matrix

$$\Lambda = \begin{pmatrix} 0 & 1 \\ 1 & 0 \end{pmatrix}. \quad (\text{C3})$$

The equations (C1) and the relations between the different spectral densities (C2) for a given sublattice ν are

formally the same as in the homogeneous case $J_1 = J_2$ (A2).

- ¹ G. R. Stewart, Rev. Mod. Phys. **73**, 797 (2001).
- ² H. v. Löhneysen, A. Rosch, M. Vojta, and P. Wölfle, Rev. Mod. Phys. **79**, 1015 (2007).
- ³ P. Gegenwart, Q. Si, and F. Steglich, Nature Phys. **4**, 186 (2008).
- ⁴ T. Goto, T. Watanabe, O. Suzuki, H. Kobayashi, Y. Nemoto, N. Takeda, A. Dönni, and H. Kitazawa, J. Phys. Soc. Jpn. **78**, 024716 (2009).
- ⁵ R. P. Deen *et al.*, Phys. Rev. B **81**, 064427 (2010).
- ⁶ H. Winkler, S. Laumann, J. Custers, A. Prokofiev and S. Paschen, Phys. Stat. Sol. B **247**, 516 (2010).
- ⁷ A. V. Gribanov, Y. D. Seropegin, and O. I. Bodak, J. Alloys Compounds **204**, L9 (1994).
- ⁸ J. Kitagawa, N. Takeda, and M. Ishikawa, J. Alloys Compounds **256**, 48 (1997).
- ⁹ The materials of the $(\text{RE})_3\text{Pd}_{20}\text{X}_6$ type crystallize in cubic $Fm\bar{3}m$ structure, with three RE ions per formula unit. Out of these, two occupy the 8c site whereas the third occupies the 4a site, such that RE ions with two distinct environments exist. Compared to the simpler two-ion model treated in the body of the paper, the Fermi-volume considerations in the regime dominated by inter-moment exchange will be different – due to the odd number of f electrons per unit cell they will be more akin to standard Kondo lattices with a single moment per unit cell – but the physics in the Kondo-dominated regime will be qualitatively similar, as two distinct screening scales exist in both cases.
- ¹⁰ N. Kimura, N. Tateiwa, M. Nakayama, H. Aoki, T. Komatsubara, T. Sakon, M. Motokawa, Y. Koike, and N. Metoki, Physica B **259-261**, 338 (1999).
- ¹¹ A. Dönni *et al.*, J. Alloys Compounds **306**, 40 (2000).
- ¹² T. Herrmannsdörfer, A. Dönni, P. Fischer, L. Keller, E. Clementyev, A. Furrer, S. Mango, B. van den Brandt, and H. Kitazawa, J. Alloys Compounds **323**, 509 (2001).
- ¹³ A. M. Strydom, A. Pikul, F. Steglich, and S. Paschen, J. Phys.: Conf. Ser. **51**, 239 (2006).
- ¹⁴ S. Paschen, M. Müller, J. Custers, M. Kriegisch, A. Prokofiev, G. Hilscher, W. Steiner, A. Pikul, F. Steglich, and A. Strydom, J. Magn. Magn. Mater. **316**, 90 (2007).
- ¹⁵ A. Prokofiev, J. Custers, M. Kriegisch, S. Laumann, M. Müller, H. Sassik, R. Svagera, M. Waas, K. Neumaier, A. M. Strydom, and S. Paschen, Phys. Rev. B **80**, 235107 (2009).
- ¹⁶ M. Vojta, Phys. Rev. B **78**, 125109 (2008).
- ¹⁷ S. Doniach, Physica B **91**, 231 (1977).
- ¹⁸ A somewhat similar “Kondo proximity effect” has been discussed for correlated heterostructures in: R. W. Helmes, T. A. Costi, and A. Rosch, Phys. Rev. Lett. **101**, 066802 (2008).
- ¹⁹ The original exhaustion argument due to Nozières [P. Nozières, Ann. Phys. Fr. **10**, 19 (1985)] was found to be incorrect within the framework of local-self energy approximation to Kondo and Anderson lattices^{20–22}, see also: P. Nozières, J. Phys. Soc. Jpn. **74**, 4 (2005). Nevertheless, the lattice Kondo temperature is found to be strongly reduced compared to the single-ion Kondo temperature in the limit of small conduction-electron band filling, in qualitative agreement with the idea of “exhaustion”.
- ²⁰ S. Burdin, A. Georges, and D. R. Grempel, Phys. Rev. Lett. **85**, 1048 (2000).
- ²¹ T. Pruschke, R. Bulla, and M. Jarrell, Phys. Rev. B, **61**, 12799 (2000).
- ²² C. Grenzacher, F. B. Anders, G. Czyczoll, and T. Pruschke, Phys. Rev. B **74**, 195119 (2006).
- ²³ A. C. Hewson, *The Kondo Problem to Heavy Fermions*, Cambridge University Press, Cambridge (1997).
- ²⁴ It has been proposed recently that, experimentally, the coherence scale of heavy fermion metals is generically set by inter-site effects, see: Y.-F. Yang, Z. Fisk, H.-O. Lee, J. D. Thompson, and D. Pines, Nature **454**, 611 (2008). In contrast, following Doniach’s arguments¹⁷ it is widely assumed that single-ion physics dominates for sufficiently large Kondo coupling; in this regime, local self-energy approximations like DMFT or Kondo slave bosons are believed to be valid. Whether this (theoretically reasonably well understood) regime is of broad experimental relevance is not known with certainty.
- ²⁵ R. K. Kaul and M. Vojta, Phys. Rev. B **75**, 132407 (2007).
- ²⁶ S. Burdin and P. Fulde, Phys. Rev. B **76**, 104425 (2007).
- ²⁷ H. Watanabe and M. Ogata, Phys. Rev. B **81**, 113111 (2010).
- ²⁸ R. Ballou, C. Lacroix, and M. D. Nunez Regueiro, Phys. Rev. Lett. **66**, 1910 (1991).
- ²⁹ Y. Motome, K. Nakamikawa, Y. Yamaji, and M. Udagawa, Phys. Rev. Lett. **105**, 036403 (2010).
- ³⁰ S. Burdin, preprint arXiv:0903.1942.
- ³¹ There are various related definitions of a scale \bar{T}_{coh} in the literature. The one proposed in Ref. 20 is chosen such that $\bar{T}_{\text{coh}} = T_K$ for a single Kondo impurity.
- ³² In the slave-boson approach, the entropy of a free moment is $2 \ln 2$ instead of $\ln 2$, due to the mean-field treatment of the Hilbert-space constraint.
- ³³ Q. Si, S. Rabello, K. Ingersent, and J. L. Smith, Nature **413**, 804 (2001).
- ³⁴ T. Senthil, S. Sachdev, and M. Vojta, Phys. Rev. Lett. **90**, 216403 (2003); T. Senthil, M. Vojta, and S. Sachdev, Phys. Rev. B **69**, 035111 (2004).
- ³⁵ I. Paul, C. Pépin, and M. R. Norman, Phys. Rev. Lett. **98**, 026402 (2007); Phys. Rev. B **78**, 035109 (2008).
- ³⁶ T. Senthil and M. Vojta, Phys. Rev. B **71**, 121102(R) (2005).